How to cite: *Angew. Chem. Int. Ed.* **2023,** *62,* e202219313
doi.org/10.1002/anie.202219313

Conducting Polymers

Blended Conjugated Host and Unconjugated Dopant Polymers Towards N-type All-Polymer Conductors and High-ZT Thermoelectrics

*Jinfeng Han, Yufeng Jiang, Emma Tiernan, Connor Ganley, Yunjia Song, Taein Lee, Arlene Chiu, Patty McGuiggan, Nicholas Adams, Paulette Clancy, Thomas P Russell, Patrick E. Hopkins, Susanna M. Thon, John D. Tovar, and Howard E. Katz**

Abstract: N-Type thermoelectrics typically consist of small molecule dopant + polymer host. Only a few polymer dopant + polymer host systems have been reported, and these have lower thermoelectric parameters. N-type polymers with high crystallinity and order are generally used for high-conductivity (σ) organic conductors. Few n-type polymers with only short-range lamellar stacking for high-conductivity materials have been reported. Here, we describe an n-type short-range lamellar-stacked all-polymer thermoelectric system with highest σ of 78 S^{-1}, power factor (PF) of 163 $\mu W m^{-1} K^{-2}$, and maximum Figure of merit (ZT) of 0.53 at room temperature with a dopant/host ratio of 75 wt%. The minor effect of polymer dopant on the molecular arrangement of conjugated polymer PDPIN at high ratios, high doping capability, high Seebeck coefficient (S) absolute values relative to σ, and atypical decreased thermal conductivity (κ) with increased doping ratio contribute to the promising performance.

Introduction

Semiconducting polymers have been used for many kinds of devices, such as organic solar cells (OSCs),[1] polymer photodetectors (PPDs),[2] thin film field effect transistors (TFTs),[3] polymer light emitting diodes (LEDs),[4] organic thermoelectric devices,[5] wearable devices,[6] photoacoustic-imaging,[7] photothermal therapy[8] and neural applications.[9] Organic thermoelectrics have attracted increasing attention because of the potential value in transforming heat energy into electricity. More than 50 % of available natural and waste heat energy is low-temperature (<250 °C) which could conceivably be recovered by organic thermoelectrics.[10] The low σ and ZT of n-type polymers are still challenges for organic thermoelectrics. The low σ is because the electron mobility and doping efficiency of n-type organic thermoelectrics are limited.[11] Matching and engineering of n-dopants and n-polymers to enhance the doping efficiency have led to some progress.[12] The values of σ and Seebeck coefficient are usually in an inverse relationship,[13] leading to the relatively low ZT (<0.2) at room temperature (r.t.)[14] which is much lower than that (ZT=0.5–1 at r.t.) of inorganic n-type materials.[15] Seebeck coefficient for a given electronic conductivity can be increased by reducing the Coulombic interaction between host and dopant[16] but is decreased by higher carrier concentrations that contribute to σ.[17]

To decrease the Coulombic interaction and increase σ, the host-dopant distance and electron mobility (μ) of doped polymers should be increased. The engineering of tailored dopants and conjugated polymers is an effective method to

[*] J. Han, Y. Song, T. Lee, P. McGuiggan, N. Adams, J. D. Tovar, H. E. Katz
Department of Materials Science and Engineering and Department of Chemistry, Johns Hopkins University
3400 North Charles Street, Baltimore, MD 21218 (USA)
E-mail: hekatz@jhu.edu

Y. Jiang, T. P Russell
Materials Sciences Division, Lawrence Berkeley National Laboratory
Berkeley, CA 94720 (USA)

E. Tiernan, P. E. Hopkins
Department of Mechanical and Aerospace Engineering, University of Virginia
Charlottesville, VA 22904 (USA)

C. Ganley, P. Clancy
Department of Chemical and Biomolecular Engineering, Johns Hopkins University
3400 North Charles Street, Baltimore, MD 21218 (USA)

A. Chiu, S. M. Thon
Department of Electrical and Computer Engineering, Johns Hopkins University
3400 North Charles Street, Baltimore, MD 21218 (USA)

P. E. Hopkins
Department of Materials Science and Engineering, University of Virginia
Charlottesville, VA 22904 (USA)
and
Department of Physics, University of Virginia
Charlottesville, VA 22904 (USA)

achieve this goal. The triaminomethane with strong hydride donating property[18] and trimethoxy-substituted 4-(1,3-dimethyl-2,3-dihydro-1*H*-benzoimidazol-2-yl)phenyl)dimethylamine (N-DMBI) (TP-DMBI)[19] dopants with larger sizes, higher singly occupied molecular orbital (SOMO) energy levels and enhanced hydride transfer[20] led to higher σ, Seebeck coefficient and power factors, associated with good dopant-host miscibility. Introducing polarizable triethylene glycol type side chains to n-polymers can promote dispersion of the dopant in the host polymers, thus increasing the doping efficiency and σ.[21]

Other efforts have been devoted to the engineering of n-polymer backbones. Some effective ways to achieve high σ include increasing lactone-benzene ring density on the backbone,[21b,22] introducing electron-withdrawing groups to donor units[23] and optimizing the acceptor units[24] within donor-acceptor (D-A) polymers. These optimized acceptor units play a key role in σ and ZT of doped films. Until now, the n-type D-A or acceptor-acceptor (A-A) linear polymers used for doped films with $\sigma \geq 10\ S\,cm^{-1}$ are mostly based on benzodifurandione-based oligo(p-phenylene vinylene) (BDOPV),[25] thiophene fused bithiophene imide (CNDTI),[26] thiazolothienyl imide (TzTI),[12a] pyrazine-flanked diketopyrrolopyrrole (PzDPP)[23b] and thiophene-fused benzodifurandione-based oligo(p-phenylenevinylene) (TBDOPV).[27] Developing new n-type polymers is still an urgent task to achieve high σ for n-type organic thermoelectrics. Our recent report suggests that a polymer dopant is effective in improving the Seebeck coefficient and ZT of n-type thermoelectrics.[28] Polymer dopants can also enhance the mechanical properties,[29] thermal stability[30] and organic solvent stability[31] of thermoelectric films. The σ of n-type all-polymer thermoelectrics with significantly high power factors are $\leq 10\ S\,cm^{-1}$, which is much lower than films doped with small molecule dopants.[32] New polymers are needed to achieve high-σ and high-ZT n-type all-polymer thermoelectrics.

To summarize our polymer design considerations, the conjugated polymer structure draws from principles in the above references. For example, the dipyrrolidinopyrrole subunit[24] is a compact electron-attracting segment. There is a minimal distance between benzo-5-membered ring carbonyls.[22] The dicyanovinyl group is obviously more electron-withdrawing than the ring oxygen in a lactone. All of these taken together lead to a polymer with high conjugation and strong electron-attracting character. As stated in detail in our previous publication,[28] the polymer dopant was designed to provide a suitable number density of fluoride dopant ions combined with styrene comonomers and alkyl side chains to confer adequate solubility and inhibit thermal conductivity. The polymer form of the dopant was also expected to add stability.

Here, we report a comparative study of a newly designed semiconducting polymer PDPIN doped with copolymer ionic dopant PSpF and molecular dopant N-DMBI (Figure 1), providing a new system for n-type all-polymer

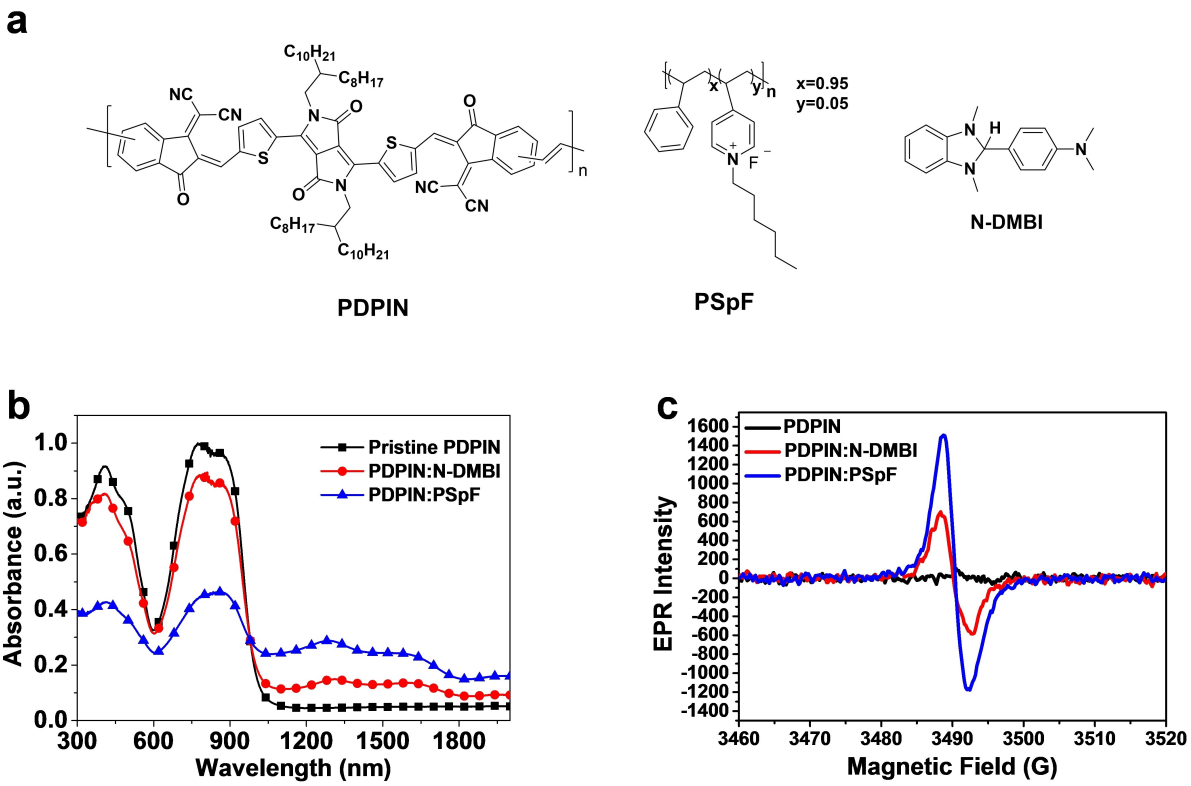

Figure 1. a) Chemical structures of polymers and dopants used in this work. b) Absorption spectra of 5 mol% N-DMBI and 75 wt% PSpF doped PDPIN films, c) EPR spectra of 5 mol% N-DMBI and 50 wt% PSpF doped PDPIN in *o*-DCB solution (50 µL). Note that spin density would be double the density of generated mobile anions, since the neutral radicals following charge transfer would also contribute to ESR peaks.

thermoelectrics with high-σ and ZT. The involvement of F- in the doping of PDPIN:PSpF was supported by energy-dispersive X-ray spectroscopy (EDS) observation and ab initio computational calculations. We observe a high σ of 78 $S\,cm^{-1}$ for an n-type all-polymer thermoelectric. The impressive maximum power factor of 163 $\mu W\,m^{-1}\,K^{-2}$ (nearly double that from a recent proton-doped high-conductivity system[12b]) and ZT of 0.53 at room temperature are achieved with relatively high S and low thermal conductivity. Ultraviolet-visible-near infrared (UV/Vis-NIR) absorbance measurements indicate that all-polymer films have stronger polar/bipolar absorption than molecular N-DMBI-doped films. A larger vacuum level shift and higher spin density in all-polymer doped films are calculated using ultraviolet photoelectron spectroscopy (UPS) and electron paramagnetic resonance (EPR) measurements. The discovery illustrates a new polymer blend architecture for high-σ conductors for plastic electronics and thermoelectrics.

Results and Discussion

PDPIN was synthesized by Stille coupling polymerization (Supporting Information Section 2). It had low lowest unoccupied molecular orbital (LUMO) energy levels of −4.26 eV (Figure S3), much lower than the singly occupied molecular orbital (SOMO) energy levels (−2.36 eV) of N-DMBI,[19] suggesting it can be doped by N-DMBI. The corresponding highest occupied molecular orbital (HOMO) energy levels calculated from the onset oxidation in the cyclic voltammetry curves is −5.55 eV (Figure S3), and the electrochemical band gap is 1.29 eV. The optical band gap of PDPIN estimated from the film absorption onset is 1.23 eV (Figure 1b), which is very close to the electrochemical band gap. The calculated HOMO and LUMO frontier orbitals of the 2,2′-((2E,2′E)-(((2,5-bis(2-octyldodecyl)-3,6-dioxo-2,3,5,6-tetrahydropyrrolo[3,4-c]pyrrole-1,4-diyl)bis(thiophene-5,2-diyl))bis(methanylylidene))bis(3-oxo-2,3-dihydro-1H-indene-2,1-diylidene))dimalononitrile (DPIN) repeat unit within PDPIN are shown in Figure S4; the calculated LUMO and HOMO energy levels are −4.2 and −5.0 eV, respectively. The electrophilicity of PDPIN, with its electron-withdrawing dicyanomethyleneindanone conjugated subunit, increased the driving force for forming the adduct of PDPIN with F^-. The weight-average molecular weight of PDPIN, 122 kDa, was measured using gel permeation chromatography (GPC) at 150 °C (Figure S5). There are three absorption peaks observed in pristine PDPIN films at 406, 776 and 866 nm, the first is from the π-π* transition and the latter two are from intramolecular charge transfer.[33] There is no absorption peak between 300–400 nm in the absorption spectra of PSpF,[28] so the absorption of π-π* transitions in PSpF-doped PDPIN films is from PDPIN. The absorption peak of N-DMBI was detected between 300–350 nm,[34] the π-π* transitions absorption peak of pristine PDPIN is 406 nm, and with the increase of N-DMBI ratio, the π-π* transitions absorption peak moved to 340 nm, so the π-π* bands of N-DMBI doped PDPIN films had contributions from both of N-DMBI and PDPIN. A new peak at 575 nm was detected in 75 mol% N-DMBI-doped PDPIN, suggesting bipolaron formation because of over-doping. The absorbance spectra at 300–1000 nm of both of N-DMBI and PSpF doped films are bleached, which is as expected and similar to other doped films.[35] After doping with 1 mol% N-DMBI, two more absorbance peaks at 1325 and 1585 nm were detected, which can be assigned to polaron/bipolaron transitions.[36] The peak at 869 nm decreases with an increasing N-DMBI/PDPIN molar ratio. PSpF-doped PDPIN films exhibit very different absorbance spectra from N-DMBI-doped films. The peak at 792 nm decreases when the PSpF/PDPIN weight ratio increases, and the peak at 869 nm presents no shift, suggesting PSpF-doped PDPIN films have stronger intramolecular charge transfer than N-DMBI-doped films (Figure S6).[37] To estimate the doping efficiency of the doped films, we calculated the ratio of absorbance peaks at 600–1000 nm ($Abs_{600\text{-}900}$) and 1250–1850 nm ($Abs_{1250\text{-}1850}$). The absorbance spectra of 5 mol% N-DMBI and 75 wt% PSpF-doped PDPIN were examined because the highest σ values occurred at these dopant/PDPIN ratios. The ratios of $Abs_{600\text{-}900}$ and $Abs_{1250\text{-}1850}$ of N-DMBI and PSpF-doped PDPIN are 5.9 and 1.6, respectively. The lower ratio of PSpF-doped PDPIN suggests a higher doping efficiency.[25]

To confirm the formation of polarons and bipolarons, and to estimate the spin density, EPR spectra of pristine and doped PDPIN were collected. The EPR intensity is initially increased when the dopant ratios increase as more single electrons are transferred to conjugated subunits (Figure S7). However, when the dopant ratio reaches 75 mol% and 100 wt% for N-DMBI and PSpF (Figure S7), respectively, the EPR intensity decreases somewhat. The spin density of 5 mol% N-DMBI and 50 wt% PSpF-doped PDPIN was calculated to be 1.8×10^{20} and $2.4\times10^{20}\,cm^{-3}$ (Figure 1e). If we assume the PDPIN radical anion is the only single electron structure, the corresponding doping efficiency of PSpF is 56 %.[38] Considering that the σ of 5 mol% N-DMBI-doped ($19.1\pm2.4\,S\,cm^{-1}$) and 50 wt% PSpF-doped PDPIN ($22.2\pm1.5\,S\,cm^{-1}$) are close, and the values of the lower doping efficiency of PSpF may be compensated by higher mobility, it can be concluded that inter-polaron distance and electron mobility both play a key role in the electron transport.[39]

The valence bands of N-DMBI- and PSpF-doped PDPIN are 4.33 and 4.16 eV, respectively, measured using UPS. The corresponding shifts from pristine PDPIN are 0.89 and 0.72 eV away from the Fermi level (Figure S8), consistent with n-doping.[39] The higher energy valence bands can lower the energy needed for electrons to reach the conduction bands.[40]

The proposed doping mechanism shown in Figure 2 was evaluated. We hypothesized that F- ions can interact with PDPIN through a stabilizing interaction (Figure 2a) IR spectra were obtained to support this step in the doping mechanism (Figure S9). For example, the IR signal at 2222 cm^{-1} (absorption peak of cyan group) was shifted to lower energy, broadened, and decreased in intensity when PDPIN was doped with PSpF, so F^- prefers to attack the dicyanomethylene group, either directly or through con-

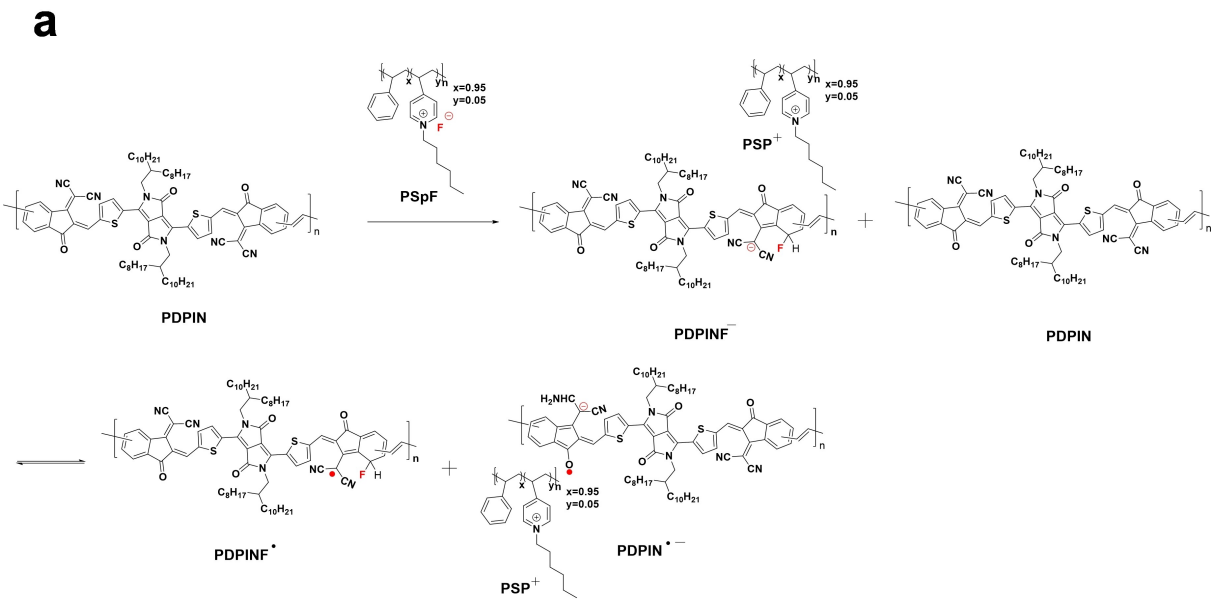

b

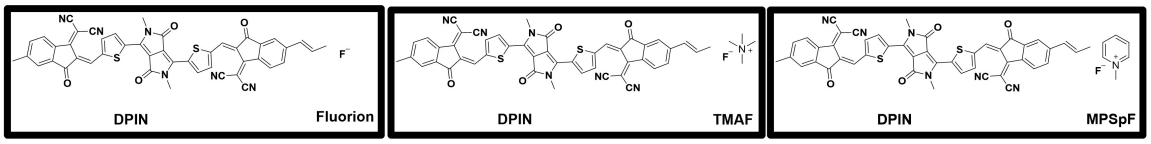

Adduct Name	DPIN-F	DPIN-TMAF	DPIN-MPSpF
Binding Energy (eV) Mean (Highest)	-0.3 (-0.6)	-0.2 (-0.4)	-0.4 (-0.7)
Electron Affinity (eV) Mean (Highest)	-3.7 (-3.8)	-3.9 (-4.0)	-3.9 (-4.0)
Ionization Energy (eV) Mean (Highest)	5.0 (5.1)	5.4 (5.7)	5.3 (5.4)

Figure 2. a) The proposed doping process of PSpF doped PDPIN. Other F^- addition sites and radical/anion resonance structures are possible. b) The calculated binding energy and electron affinity of adducts of F^-, TMAF (model molecule of TBAF) and MPSpF (model molecule of PSpF) associated with DPIN. The DPIN LUMO energy level is −4.2 eV (Figure S4).

jugated double bonds. Other IR shifts on doping are listed in the Supporting Information accompanying Figure S9.

To further study the doping reaction, density functional theory (DFT) calculations were performed using the ORCA software package.[41] A uniform dielectric constant was applied to the simulation medium (i.e. an "implicit solvent"), via the conductor-like polarizable continuum model (CPCM), to emulate the presence of orthodichlorobenzene, the solvent used in experiments. The DPIN repeat unit of PDPIN was used as a model compound to react with F^-. TMAF and MPSpF were used as model compounds of TBAF and PSpF, respectively. All adducts of DPIN-F, DPIN-TMAF and DPIN-MPSpF present similar ionization energy of 5.0–5.7 eV (Table S1–3). This is the ionization that leads to doping of other, nonfluorinated DPIN subunits. The average binding (interaction stabilization) energy and electron affinity of the adduct of DPIN and F^- are −0.3 and −3.7 eV (Figure 2b). The average binding energy and electron affinity of DPIN-TMAF were calculated to be −0.2 and −3.9 eV (Figure 2b). As mentioned above, the electron affinity of nonfluorinated DPIN is −4.2 eV, and it would presumably be higher if it were associated with a counter cation. The counter-cation TMA^+ seemingly contributes little to the formation stability of DPIN- TMAF. Compared with DPIN-TMAF, the electron affinity of DPIN-MPSpF does not change, the average binding energy of DPIN-

MPSpF is increased to −0.4 eV (Figure 2b) and the highest binding energy absolute values increases from 0.4 eV to 0.7 eV. The larger absolute value of the binding energy of DPIN-MPSpF suggests $MPSpF^+$ has a better capability to stabilize the adduct, and it would also stabilize a radical anion formed by doping. The geometry optimizations of DPIN-MPSpF with a binding energy of −0.7 eV show that the counter ion of piperidine is mainly located between the backbones of PDPIN (Figure S2d), which is consistent with the results of 2D GIWAXS.

The thermoelectric performance of PDPIN films doped by N-DMBI and PSpF was explored by measuring drop-cast films in open air. As shown in Figure 3a, the σ increases when the PSpF/PDPIN ratios increase from 5 wt% to 75 wt %. The σ (maximum followed by mean and standard deviation in parentheses) of 10.5 (9.5±1), 15.5 (12.3±3.2), 26.3 (23.4±2.9), and 78.1 (67.1±11.1) $S\,cm^{-1}$ were recorded at ratios of 5, 30, 50 and 75 wt% (Table 1), respectively. It is worth noting that 75 wt% PSpF doped PDPIN presented the highest σ of 78 $S\,cm^{-1}$, a breakthrough for n-type all-polymer conductors intended for thermoelectrics. The relatively high conductivity can be attributed to high doping efficiency, high mobility and little disordering caused by PSpF (Figure 6). The conductivity is much higher than for PSpF-doped PFClTVT,[28] perhaps because the conjugation of adduct PFClTVT-PSpF is weakened and the conjugation of adduct PDPIN-PSpF is enhanced. When the PSpF/PDPIN ratio increases to 100 wt%, σ decreases to 50 (40±10) $S\,cm^{-1}$ (Figure 3a), due to the lower ordering and larger π-π stacking distance caused by a higher proportion of dopant PSpF. N-DMBI-doped polymers have generally shown higher σ compared to other dopants.[28,42] From Figures 3 and 6, we suggest that N-DMBI-doped PDPIN films have lower σ, because the polymer molecular stacking was disordered by N-DMBI when the N-DMBI ratio was over 5 mol% (Figure 3, 6). The highest σ value of 19.1±5.3 $S\,cm^{-1}$ was achieved in a N-DMBI ratio of 5 mol%; the σ decreased to 10.6 and 1.1 $S\,cm^{-1}$ for 30 and 50 mol% N-DMBI-doped PDPIN, respectively (Figure 3d). The average absolute negative S values of PSpF-doped PDPIN decrease gradually from 206±16 to 84±10 $\mu V\,K^{-1}$ as the PSpF ratio increases from 5 to 100 wt% (Figure 3b). Though the

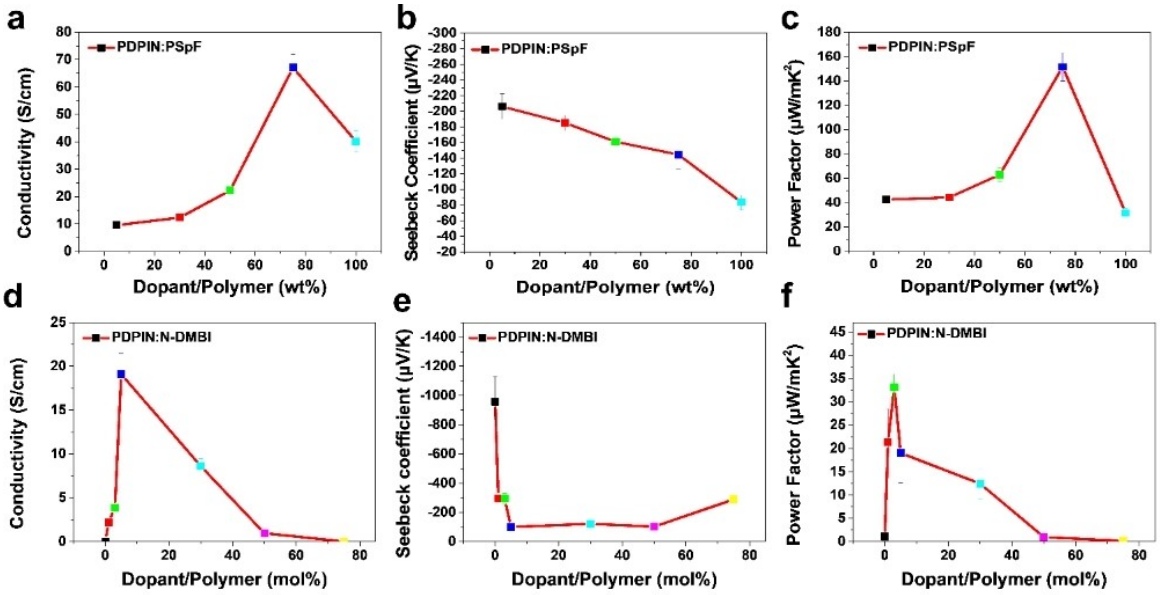

Figure 3. The electrical conductivity of a) PSpF and d) N-DMBI doped PDPIN. The Seebeck coefficient of b) PSpF and e) N-DMBI doped PDPIN. The power factor of c) PSpF and f) N-DMBI doped PDPIN.

Table 1: Performance of doped polymer films.

Polymer films	κ $W\,m^{-1}\,K^{-1}$	σ $S\,cm^{-1}$	S $\mu V\,K^{-1}$	PF $\mu W\,m^{-1}\,K^{-2}$	ZT (r.t.)
PDPIN:5 mol% N-DMBI	0.12±0.02	19.1±5.3	−100±14	19.0±6.3	0.047±0.016
PDPIN:50 mol% N-DMBI	0.15±0.02	1±0.1	−102±12	1.0±0.2	0.002±0.0004
PDPIN:5 wt% PSpF	0.20±0.03	9.5±1	−206±16	42.5±2.0	0.06±0.003
PDPIN:30 wt% PSpF	0.17±0.02	12.3±3.2	−185±10	44.2±2.1	0.08±0.004
PDPIN:50 wt% PSpF	0.12±0.02	23.4±2.9	−161±4	62.9±5.4	0.16±0.01
PDPIN:75 wt% PSpF	0.093±0.01	67.1±11.1	−145±19	151.5±11.5	0.49±0.04
PDPIN:100 wt% PSpF	0.16±0.02	40.1±10.4	−84±10	31.6±3.6	0.06±0.007

absolute value of S of PSpF-doped PDPIN is relatively high, it remains very reasonable and very close to the trend of other p-type and n-type organic thermoelectric materials (Figure S10).[5] It is very difficult to achieve the highest σ and power factor simultaneously because the absolute values of S usually decrease when σ increases.[22,43] Here, the absolute S values of PSpF-doped PDPIN decrease relatively slowly when σ increases; 75 wt% PSpF-doped PDPIN presents the highest σ and power factor simultaneously, which is very rare and useful for thermoelectrics. The highest power factors are 163 (145 ± 19) $\mu W m^{-1} K^{-2}$ at room temperature, among the best results reported for organic thermoelectrics (Figure 3c). Moreover, high power factors of 44 (42.5 ± 2), 46 (44.2 ± 2.1), 68 (62.9 ± 5.4) and 35 (31.6 ± 3.6) $\mu W m^{-1} K^{-2}$ were achieved at PSpF ratios of 5, 30, 50, and 100 wt% (Table 1), respectively. All these values are also very high for organic thermoelectrics, showing that PDPIN appears particularly well-suited for use with the polymer dopant PSpF. For N-DMBI-doped films, 3 mol% N-DMBI-doped PDPIN shows the highest power factor of 36 (33.1 ± 2.9) $\mu W m^{-1} K^{-2}$ (Figure 3f), with a corresponding σ of 4 (3.8 ± 0.3) $S cm^{-1}$ (Figure 3d). The power factor of doped films with 5 and 30 mol% N-DMBI ratios are 25 (19 ± 6.3) and 16 (12.4 ± 3.3) $\mu W m^{-1} K^{-2}$ (Figure 3f), respectively. The power factor values are, again, among the best results of N-DMBI-doped polymers,[11] suggesting PDPIN is a promising polymer for n-type organic thermoelectrics.

The higher S values of PSpF-doped PDPIN relative to its σ can be attributed to the larger distance between counter-cation and -anion,[16a] which is caused by the large polymer molecule size of PSpF. To further confirm this hypothesis, we measured PDPIN films doped with TBAF, which has a much smaller volume per dopant molecule. Although 30 mol% TBAF-doped PDPIN presents the highest σ of 24 $S cm^{-1}$, the corresponding power factor is only 5.6 $\mu W m^{-1} K^{-2}$ (Figure S11), which is much lower than that of N-DMBI and PSpF doped films with similar σ values. The S values at similar σ levels are summarized in Figure 4a and b. When σ is about 10 $S cm^{-1}$, S for PSpF and N-DMBI-doped PDPIN are -206 and -122 $\mu V K^{-1}$, respectively;

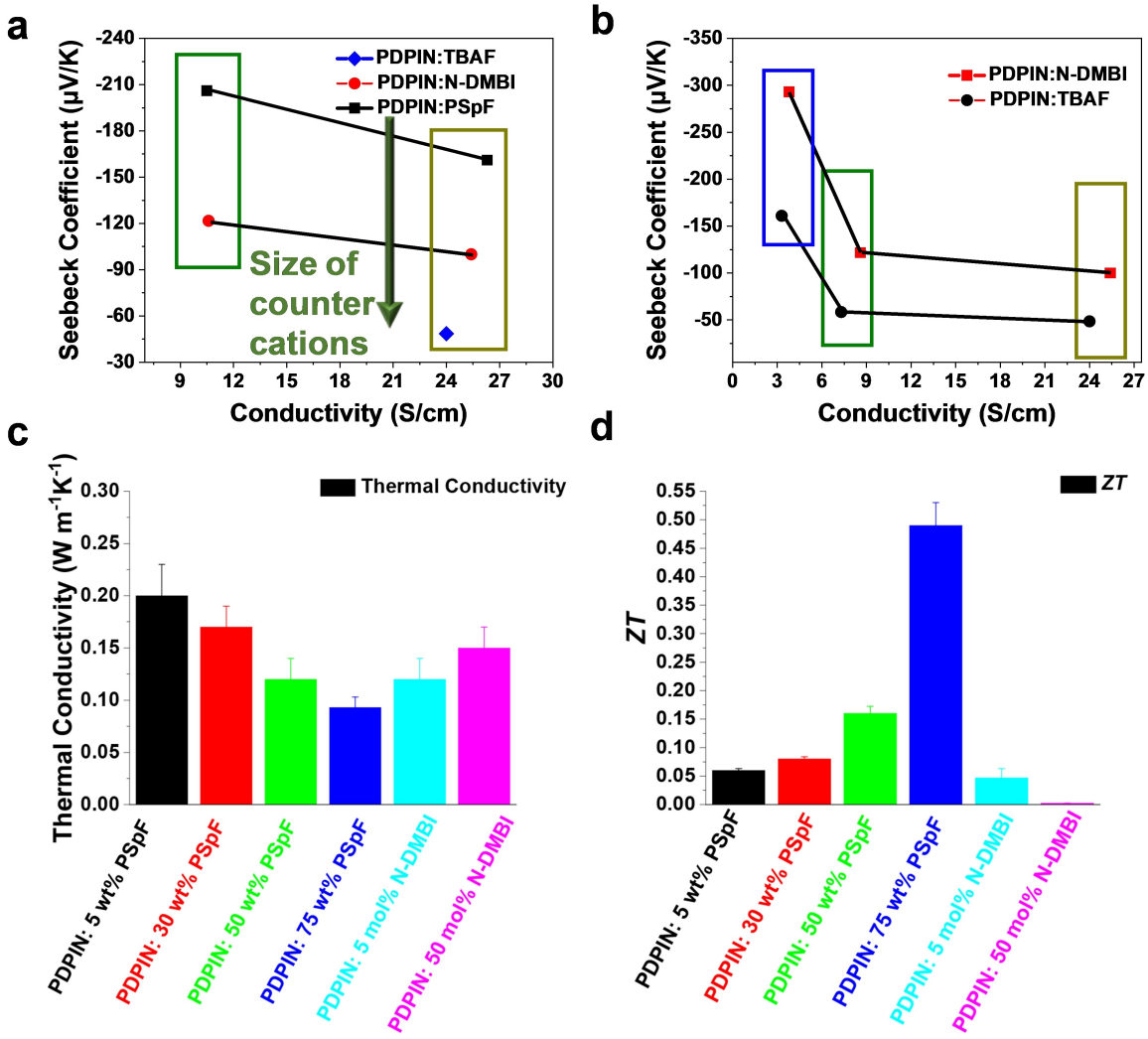

Figure 4. a) The Seebeck coefficient of TBAF, N-DMBI and PSpF doped PDPIN at similar electrical conductivity levels. b) The Seebeck coefficient of TBAF and N-DMBI doped PDPIN at similar electrical conductivity levels. c) The thermal conductivity and d) ZT of N-DMBI and PSpF doped films.

When σ is about 25 S cm^{-1}, S values of PSpF-, N-DMBI- and TBAF-doped PDPIN are −161, −100 and −49 μV K^{-1}, respectively. These absolute values decrease when the size of the counter-cations decrease, probably due to the fact that the sizes of counter-cations play a key role in determining host-dopant distances and further affect the Coulombic interaction.[16a] S of N-DMBI- and TBAF-doped PDPIN at σ levels of about 3 and 7 S cm^{-1} also follow the same trend (Figure 4b). Raw ΔV-T plots are provided in Figure S12 and 13, which show high linearity (Figure S13). To further confirm that the major contribution to S is due to electron, rather than ion, redistribution, time-dependent thermal voltage responses of N-DMBI and PSpF-doped PDPIN were recorded. As shown in Figure S14, the thermal voltages of PSpF-doped PDPIN at different temperature gradients are stable; this result is similar to that of N-DMBI-doped PDPIN films. Though 5 mol% N-DMBI and 75 wt% PSpF-doped PDPIN have different σ values, the activation energy is similar, being 181 and 186 meV (Figure S14c,d), respectively.

As a final check whether the high σ and S values for PSpF-doped PDPIN arises from electron transport, we recorded the time (1 h)-dependent current through 75 wt% PSpF-doped PDPIN with an application of −50 V (Figure S15). The current is fairly stable over one hour, suggesting electron transport contributes to the high σ. The mean current is 1.65 milliamps: 3600 seconds × 1.65 milliamps which equates to 5.94 coulombs, or 3.7×10^{19} electrons; this would be 6.2×10^{-5} moles. A typical polymer density is generally about 1–1.1 g cm^{-3},[44] with polystyrene specifically about 1 g cm^{-3}.[45] Thus, the volume of a mole of PDPIN repeat units plus the dopant PSpF is about 1430 cm^3. The 6.2×10^{-5} moles should have a volume of 0.09 cm^3. However, the real volume of doped films is below 10^{-4} cm^3, so there are many more moving charges than ions in the PSpF-doped PDPIN film, further revealing the all-electronic transport in the film.

Thermal conductivity measurements were undertaken to determine the figure of merit of doped films. The films are presumed to be isotropic, as GIWAXS measurements discussed below showed no signs of orientation. The thermal conductivity decreases when the ratio of PSpF increases from 5 wt% to 75 wt% (Figure 4c). The average thermal conductivity values are 0.21, 0.16, 0.13 and 0.099 W m^{-1} K^{-1} for 5, 30, 50 and 75 wt% PSpF doped films (Table 1). When the ratio of PSpF/PDPIN is 100 wt%, the thermal conductivity increases to 0.16 W m^{-1} K^{-1}. It is interesting to note that the films of 75 wt% PSpF-doped PDPIN present the highest σ, power factor and lowest thermal conductivity among PSpF-doped films, giving a record-breaking maximum ZT (0.53 at room temperature) among n-type all-polymer thermoelectrics (Figure 4d), which is comparable with that of n-type inorganic thermoelectrics at room temperature.[15] The calculated highest ZT (means and standard deviations follow) of 5, 30 and 50 wt% PSpF-doped PDPIN are 0.063 (0.06±0.003), 0.087 (0.08±0.004) and 0.17 (0.16±0.01) (Table 1), respectively. The values are also substantial compared to recently reported n-type organic thermoelectrics.[14b] The highest Figures of merit of 5 and 50 mol% N-DMBI-doped PSpF are 0.063 (0.047±0.016) and 0.0024 (0.002±0.0004) (Table 1), respectively, which are much lower than those of PSpF doped films, further demonstrating the potential and advantage of PSpF.

The air stability of doped PDPIN films is studied by recording σ at 0, 25, 50 and 75 days after storing in ambient conditions. PSpF-doped PDPIN presents much higher air stability of σ than that of N-DMBI-doped PDPIN (Figure 5). Usually n-type organic thermoelectric materials are only stable when the films are microns thick,[18] and few works report air stability beyond 10 days. Here, we observed the stability of doped films with nanometer thickness after exposure to air over two months. The initial σ can be defined as σ_0, and σ after 75 days can be defined as σ_{75}. In the first 25 days, σ of 75 wt% PSpF- and 5 mol% N-DMBI-doped PDPIN decreased by 43% and 84% (Figure 5a, d), respectively. PSpF-doped films not only exhibit higher σ, but also have much better performance than that of N-DMBI-doped films, suggesting the PSpF is very suitable dopant for polymer PDPIN. The reduction of the mean values of σ for 75 wt% PSpF-doped PDPIN at 50 and 75 days (σ_{75}) are 31% and 9%, respectively. Even then, both of the highest σ at 50 and 75 days are 27.4 S cm^{-1}, suggesting an excellent long-term air stability. The corresponding decreases of 5 mol% N-DMBI-doped PDPIN are 47% and 53%, suggesting thin films of N-DMBI-doped films cannot form effective self-encapsulated structures as previously hypothesized for thick films.[22] The S absolute values of 75 wt% PSpF-doped PDPIN change little; and the values for 5 mol% N-DMBI-doped PDPIN increase with time delay (Figure 5b**, e**). It is very interesting that the decrease of σ decreases with an increase in PSpF weight ratio (Figure 5g). The decreases of 5, 30, 50, 75 and 100 wt% PSpF-doped PDPIN after 75 days are 95%, 84%, 77%, 67% and 64%, respectively. These results further confirm that PSpF plays a key role in the stability of doped PDPIN: the abundant polystyrene fragments can prevent water and oxygen from diffusing into the doped films. The decreases of 5, 30, and 50 mol% N-DMBI-doped PDPIN are 96%, 98% and 99% **(**Figure 5j); they are much higher than that of PSpF doped films and increase along with the molar ratio of N-DMBI, suggesting that N-DMBI may play a destructive role in stability of doped films. The initial power factor can be defined as PF_0, and the power factor after 75 days can be defined as PF_{75}. The S absolute values of 5, 30, 50, and 100 wt% PSpF-doped PDPIN increase with time delay (Figure S16–19). On the other hand, σ decreases over time. The corresponding percent decreases of power factors after 75 days are 52%, 21%, 51%, and −117% (an increase!) (Figure 5h), respectively. It is surprising that the power factors of 100 wt% PSpF-doped PDPIN did not decrease, but instead increased to a value of 90 μW m^{-1} K^{-2} because of the relatively low decrease of σ and higher increase of S values (Figure S19). Although S absolute values of N-DMBI-doped PDPIN also increased with time delay (Figure S20, 21), the decreases of σ values are so high that the power factors dropped drastically. The decrease of 5, 30 and 50 mol% N-DMBI-doped PDPIN are about 90% (Figure 5k) which is much higher than that of PSpF-doped

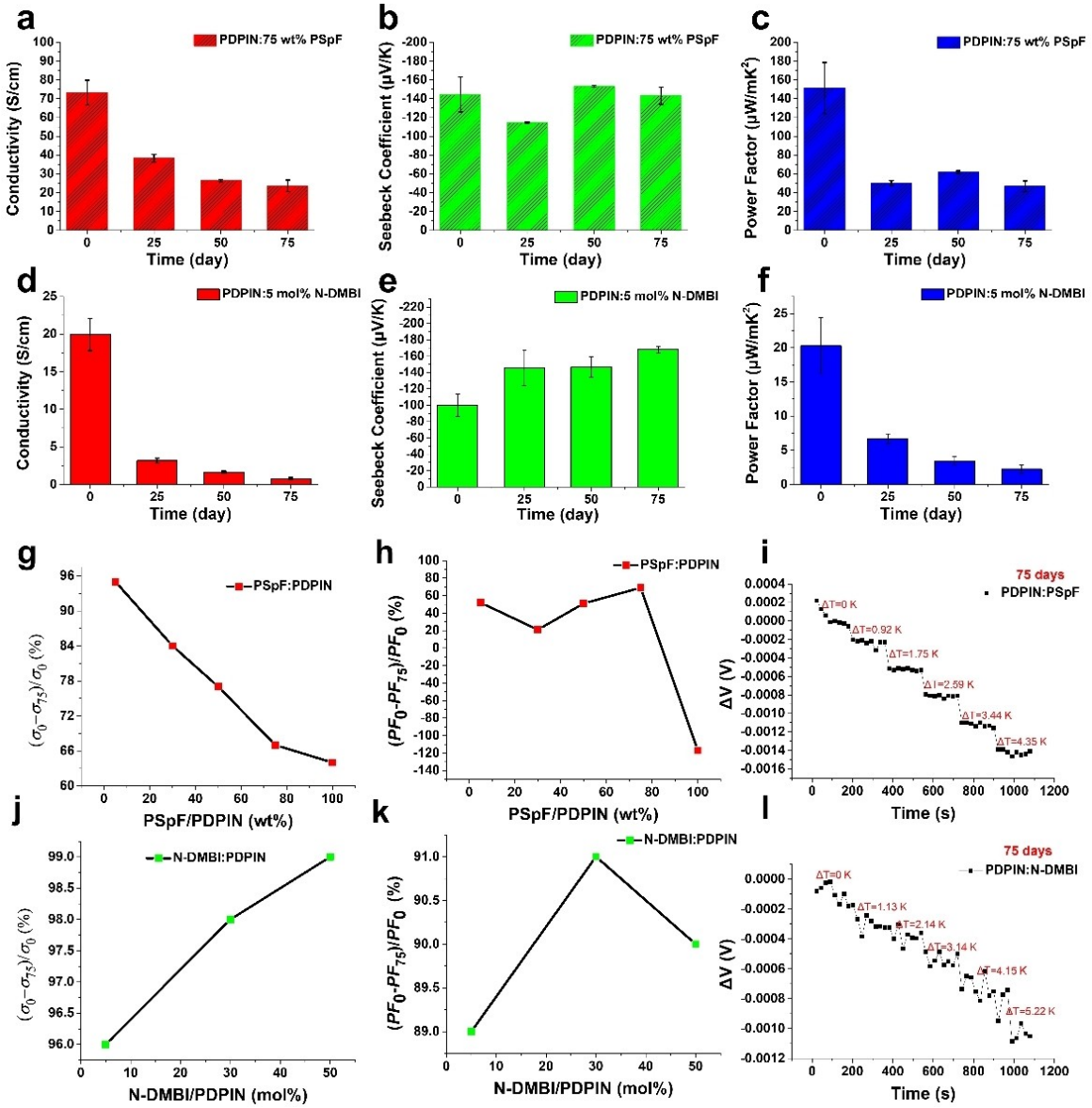

Figure 5. Air stability of a) electrical conductivity, b) Seebeck coefficient and c) Power factor of 75 wt% PSpF doped PDPIN films. Air stability of d) electrical conductivity, e) Seebeck coefficient and f) Power factor of 5 mol% N-DMBI doped PDPIN. The change of g) electrical conductivity and h) power factor of PSpF doped PDPIN after 75 days relative to initial conductivity. The time-dependent thermoelectric potential responses of i) 75 wt % PSpF and l) 5 mol% N-DMBI doped PDPIN films. The change of j) electrical conductivity and k) power factor of N-DMBI doped PDPIN after 75 days relative to initial conductivity.

PDPIN. To further check the stability of doped films, we explored time-dependent voltage response measurements. Both the N-DMBI- and PSpF-doped PDPIN films present stable voltage responses after 50 days, even more stable than the initial devices because of increased S absolute values. After 75 days, the time-dependent voltage response of N-DMBI-doped films became unstable, perhaps because of the lower σ. The stability of PSpF-doped PDPIN hardly changes after 75 days compared with that of the initial devices.

The morphology and molecular packing of films can help us further understand the underlying doping mechanism and characteristics. Here, atomic force microscopy (AFM), grazing-incidence wide-angle X-ray scattering (GIWAXS) and (scanning electron microscope) SEM measurements were performed to examine the doped films. As shown in Figure 6 and Figures S20 and S21, the polymer PDPIN presents low crystallinity and low-intensity lamellar stacking. The low order of lamellar stacking of PDPIN did not affect the high σ values of doped films, suggesting highly ordered lamellar stacking is not necessary for n-type organic conductors.[32] After doping with N-DMBI or PSpF, all of the lamellar stacking peaks are detected at $q_{xy}=0.233$ Å^{-1}, resulting in a distance of 26.97 Å, suggesting that the dopant molecules have no effect on the lamellar stacking of PDPIN and indicating that some intercalation of dopant segments occurs within the backbone parts of the conjugated

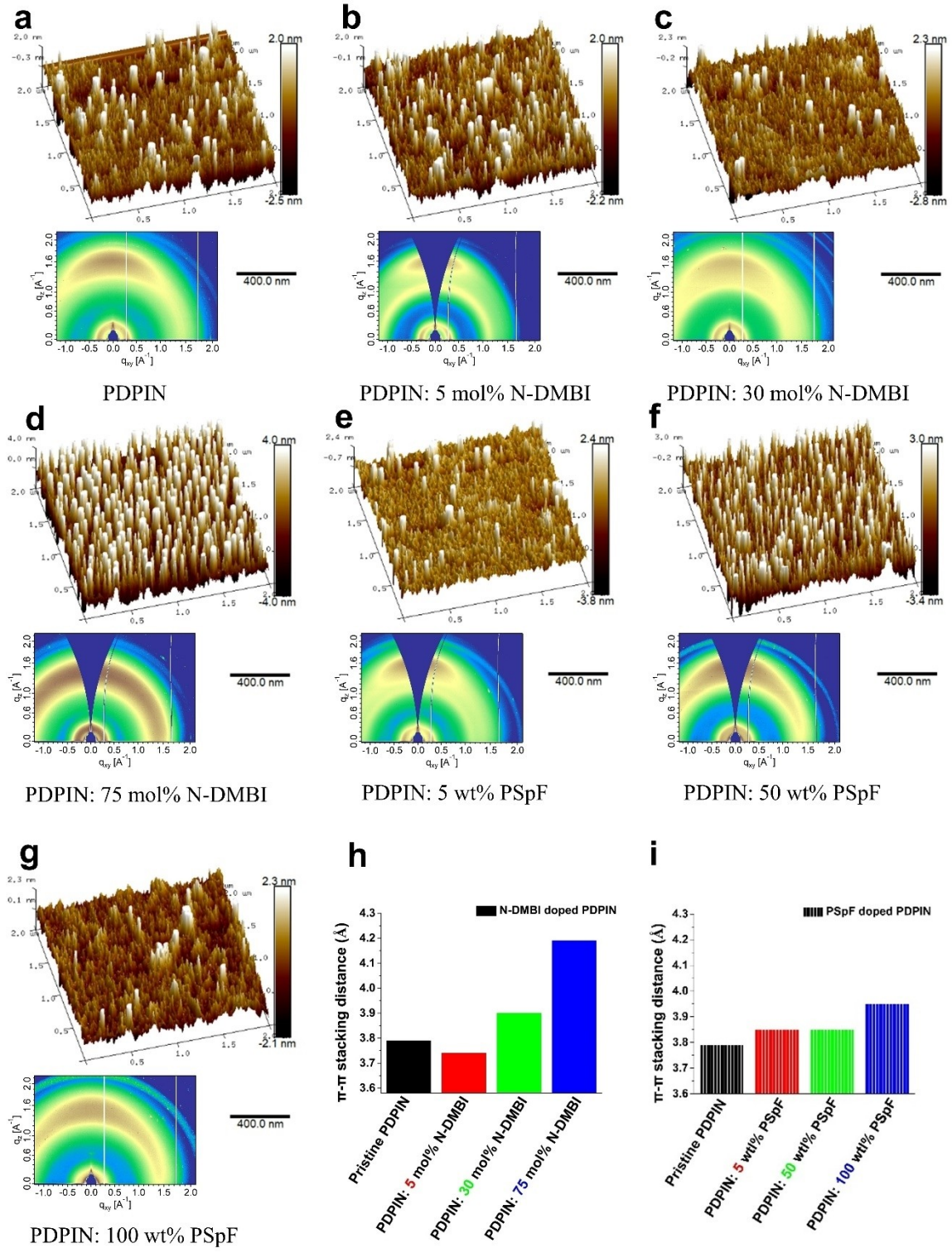

Figure 6. AFM height images and GIWAXS pattern of a) pristine PDPIN, b) 5, c) 30 and d) 75 mol% N-DMBI doped PDPIN films. AFM height images and GIWAXS pattern of e) 5, f) 50 and g) 100 wt% PSpF doped PDPIN films. The π-π stacking distance of h) N-DMBI and i) PSpF doped PDPIN films.

polymers.[46] There was no (010) peak detected in the in-plane diffractions of pristine and doped PDPIN films, which reveals that PDPIN films tend to have a face-on orientation packing with a π-π stacking distance of 3.79 Å. Figure 6b, c and d show a significant effect of N-DMBI on the molecular arrangement of PDPIN molecules: the diffraction intensity of π-π stacking was reduced when the N-DMBI molar ratio increased. After doping with 5 mol% N-DMBI, the π-π

stacking distance slightly decreased to 3.74 Å, indicating that N-DMBI has good miscibility at low molar ratio. When the N-DMBI molar ratio increased further, the π-π stacking distance increased significantly, 30 and 75 mol% N-DMBI-doped PDPIN have π-π stacking distances of 3.90 and 4.19 Å (Figure 6h), respectively. It is interesting that PSpF has a much smaller effect on the π-π stacking, and the diffraction intensity hardly changes after doping with PSpF. The π-π stacking distances are 3.85, 3.85 and 3.95 Å for 5, 50 and 100 wt% PSpF-doped PDPIN films (Figure 6i), suggesting that PSpF may have better miscibility with PDPIN at high weight or molar ratios. 5 mol% N-DMBI-doped PDPIN presents a root-mean-square (RMS) roughness of 0.74 nm which is much lower than that of pristine PDPIN films (2.16 nm), again suggesting N-DMBI has a good miscibility with PDPIN at this ratio, which is consistent with the result of the GIWAXS measurement. However, when the N-DMBI molar ratio increases to 30 and 75 mol%, the RMS roughness increases to 1.28 and 2.35 nm, respectively. The results reveal that N-DMBI can self-aggregate at high concentrations,[27] which can be confirmed by the AFM phase images (Figure S27) and EDS measurement. The spot labeled "4″ in Figure S26b and Table S11 has a higher percentage of element N than other areas and can be attributed to the aggregation of N-DMBI. Also, numerous discontinuous columnar structures in 75 mol% N-DMBI-doped PDPIN films may be another reason for the much lower σ. The RMS roughness are 1.25, 1.33, and 0.65 nm for 5, 50, and 100 wt% PSpF-doped PDPIN films. All the roughness values are much lower than for pristine PDPIN, especially for 100 wt% PSpF-doped PDPIN, suggesting that PSpF has good miscibility with PDPIN, which can be confirmed by AFM phase images (Figure S28). Our previous report suggests that F cannot be detected in EDS measurement for pristine PSpF films because F^- can escape as HF and other compounds in high vacuum.[28] In contrast, after doping with conjugated polymers, F can now be detected because of the high bond energy of covalent bonds. Here, we detected the F element in the 5, 30, 50, 75, and 100 wt% PSpF doped PDPIN films, and found that the content of F is enhanced when the PSpF ratio increases. These results further confirm our speculation regarding the doping reactions. We also found that the distribution of element F is not uniform in EDS measurement (Figure S25 and Table S4–9) because some PDPIN molecules have no F atoms (Figure 2a), indicating the formation of aggregates and phase separation of doped PDPIN molecules. This phenomenon has no effect on the electron transport because all the doped PDPIN molecules are potentially conductive.

To further explore the effect of doping on the electron transport of films, thin film transistors with a top-gate bottom-contact (TGBC) configuration were prepared and studied (Figure S29–33). The pristine PDPIN thin films present an electron mobility of 0.01 $cm^2 V^{-1} s^{-1}$, lower than other n-type polymers with higher crystallinity[47] because of the slightly disordered molecular arrangement. The lower/higher mobility of pristine films does not mean that the polymer cannot achieve higher/lower σ at high doping concentrations, because the ordered arrangement of molecules will be disordered by dopants. The electron mobility is enhanced to 0.11 $cm^2 V^{-1} s^{-1}$ after doping with 0.2 mol% N-DMBI, suggesting the effective doping reaction occurred. On the other hand, the electron mobility of 2 mol% N-DMBI-doped PDPIN decreased to 0.0035 $cm^2 V^{-1} s^{-1}$ maybe because of disordering caused by N-DMBI. The electron mobility of 0.5 wt% PSpF-doped PDPIN increases to 0.071 $cm^2 V^{-1} s^{-1}$, and 5 wt% PSpF-doped PDPIN present a much higher electron mobility of 0.42 $cm^2 V^{-1} s^{-1}$. These results further suggest that PSpF has a strong capability to dope PDPIN and hardly affects the polymer molecular arrangement.

Conclusion

N-type all-polymer organic conductors and thermoelectrics with high electrical conductivity and *ZT* have been demonstrated. Highest electrical conductivity of 78 S^{-1}, *PF* of 163 $\mu W m^{-1} K^{-2}$ and maximum *ZT* of 0.53, and lowest thermal conductivity of 0.09 $W m^{-1} K^{-1}$ were achieved at the same dopant/host ratio for PSpF doped PDPIN films. The excellent doping performance of all-polymer films was confirmed by UV/Vis-NIR absorption spectra, EPR spectra, UPS spectra and EDS measurement, associated with DFT calculations. The relatively higher doping capacity of the polymer dopant is accompanied by higher electron mobility of doped thin film transistors. Polymer dopant PSpF induces only a minor effect on the molecular arrangement of host polymer molecules, and the remarkable dopant-host miscibility of PSpF doped PDPIN at high dopant ratio were shown by 2D GIWAXS, AFM, and SEM measurements. It is also confirmed that dopant counter cations with larger sizes can result in higher absolute *S* values. Moreover, the doped films of PSpF:PDPIN system exhibit much better air stability than N-DMBI-doped PDPIN films. Our discovery will promote the development of flexible energy devices and conductors.

Supporting Information

Supporting Information is available from the Wiley Online Library or from the author.

Acknowledgements

This work was primarily supported by the National Science Foundation, Division of Chemistry, grant numbers 1708245 and 2107360. We thank Baixiang Li for the help with GPC measurement. We also appreciate support from the Office of Naval Research, grant number N00014-20-1-2686 for thermal conductivity measurements.

Conflict of Interest

The authors declare no conflict of interest.

Data Availability Statement

The data that support the findings of this study are openly available in Johns Hopkins University Data Archive at https://archive.data.jhu.edu/dataverse/root?q=, reference number 216.

Keywords: All-Polymer Thermoelectrics · Electrical Conductivity · Power Factor · Semiconducting Polymer · ZT

[1] C. Liu, K. Wang, X. Gong, A. J. Heeger, *Chem. Soc. Rev.* **2016**, *45*, 4825–4846.

[2] F. P. García de Arquer, A. Armin, P. Meredith, E. H. Sargent, *Nat. Rev. Mater.* **2017**, *2*, 16100.

[3] M. Li, J. Wang, W. Xu, L. Li, W. Pisula, R. A. J. Janssen, M. Liu, *Prog. Polym. Sci.* **2021**, *117*, 101394.

[4] A. Ren, H. Wang, W. Zhang, J. Wu, Z. Wang, R. V. Penty, I. H. White, *Nat. Electron.* **2021**, *4*, 559–572.

[5] B. Russ, A. Glaudell, J. J. Urban, M. L. Chabinyc, R. A. Segalman, *Nat. Rev. Mater.* **2016**, *1*, 16050.

[6] T. R. Ray, J. Choi, A. J. Bandodkar, S. Krishnan, P. Gutruf, L. Tian, R. Ghaffari, J. A. Rogers, *Chem. Rev.* **2019**, *119*, 5461–5533.

[7] S. Y. Ong, C. Zhang, X. Dong, S. Q. Yao, *Angew. Chem. Int. Ed.* **2021**, *60*, 17797–17809.

[8] F. Pierini, P. Nakielski, O. Urbanek, S. Pawłowska, M. Lanzi, L. De Sio, T. A. Kowalewski, *Biomacromolecules* **2018**, *19*, 4147–4167.

[9] I. B. Dimov, M. Moser, G. G. Malliaras, I. McCulloch, *Chem. Rev.* **2022**, *122*, 4356–4396.

[10] M. Massetti, F. Jiao, A. J. Ferguson, D. Zhao, K. Wijeratne, A. Würger, J. L. Blackburn, X. Crispin, S. Fabiano, *Chem. Rev.* **2021**, *121*, 12465–12547.

[11] Y. Lu, J.-Y. Wang, J. Pei, *Chem. Mater.* **2019**, *31*, 6412–6423.

[12] a) H. Guo, C.-Y. Yang, X. Zhang, A. Motta, K. Feng, Y. Xia, Y. Shi, Z. Wu, K. Yang, J. Chen, Q. Liao, Y. Tang, H. Sun, H. Y. Woo, S. Fabiano, A. Facchetti, X. Guo, *Nature* **2021**, *599*, 67–73; b) H. Tang, Y. Liang, C. Liu, Z. Hu, Y. Deng, H. Guo, Z. Yu, A. Song, H. Zhao, D. Zhao, Y. Zhang, X. Guo, J. Pei, Y. Ma, Y. Cao, F. Huang, *Nature* **2022**, *611*, 271–277.

[13] J. Gainza, F. Serrano-Sánchez, M. Gharsallah, F. Carrascoso, J. Bermúdez, O. J. Dura, F. J. Mompean, N. Biskup, J. J. Meléndez, J. L. Martínez, J. A. Alonso, N. M. Nemes, *J. Appl. Phys.* **2019**, *126*, 045105.

[14] a) J. Liu, B. van der Zee, R. Alessandri, S. Sami, J. Dong, M. I. Nugraha, A. J. Barker, S. Rousseva, L. Qiu, X. Qiu, N. Klasen, R. C. Chiechi, D. Baran, M. Caironi, T. D. Anthopoulos, G. Portale, R. W. A. Havenith, S. J. Marrink, J. C. Hummelen, L. J. A. Koster, *Nat. Commun.* **2020**, *11*, 5694; b) Y. Sun, C.-A. Di, W. Xu, D. Zhu, *Adv. Electron. Mater.* **2019**, *5*, 1800825.

[15] J. Wei, L. Yang, Z. Ma, P. Song, M. Zhang, J. Ma, F. Yang, X. Wang, *J. Mater. Sci.* **2020**, *55*, 12642–12704.

[16] a) J. Liu, G. Ye, H. G. O. Potgieser, M. Koopmans, S. Sami, M. I. Nugraha, D. R. Villalva, H. Sun, J. Dong, X. Yang, X. Qiu, C. Yao, G. Portale, S. Fabiano, T. D. Anthopoulos, D. Baran, R. W. A. Havenith, R. C. Chiechi, L. J. A. Koster, *Adv. Mater.* **2021**, *33*, 2006694; b) T. J. Aubry, K. J. Winchell, C. Z. Salamat, V. M. Basile, J. R. Lindemuth, J. M. Stauber, J. C. Axtell, R. M. Kubena, M. D. Phan, M. J. Bird, A. M. Spokoyny, S. H. Tolbert, B. J. Schwartz, *Adv. Funct. Mater.* **2020**, *30*, 2001800; c) T. J. Aubry, J. C. Axtell, V. M. Basile, K. J. Winchell, J. R. Lindemuth, T. M. Porter, J.-Y. Liu, A. N. Alexandrova, C. P. Kubiak, S. H. Tolbert, A. M. Spokoyny, B. J. Schwartz, *Adv. Mater.* **2019**, *31*, 1805647.

[17] C. Dun, C. A. Hewitt, H. Huang, J. Xu, C. Zhou, W. Huang, Y. Cui, W. Zhou, Q. Jiang, D. L. Carroll, *Nano Energy* **2015**, *18*, 306–314.

[18] C.-Y. Yang, Y.-F. Ding, D. Huang, J. Wang, Z.-F. Yao, C.-X. Huang, Y. Lu, H.-I. Un, F.-D. Zhuang, J.-H. Dou, C.-a. Di, D. Zhu, J.-Y. Wang, T. Lei, J. Pei, *Nat. Commun.* **2020**, *11*, 3292.

[19] J. Han, A. Chiu, C. Ganley, P. McGuiggan, S. M. Thon, P. Clancy, H. E. Katz, *Angew. Chem. Int. Ed.* **2021**, *60*, 27212–27219.

[20] S. Jhulki, H.-I. Un, Y.-F. Ding, C. Risko, S. K. Mohapatra, J. Pei, S. Barlow, S. R. Marder, *Chem* **2021**, *7*, 1050–1065.

[21] a) J. Liu, L. Qiu, R. Alessandri, X. Qiu, G. Portale, J. Dong, W. Talsma, G. Ye, A. A. Sengrian, P. C. T. Souza, M. A. Loi, R. C. Chiechi, S. J. Marrink, J. C. Hummelen, L. J. A. Koster, *Adv. Mater.* **2018**, *30*, 1704630; b) A. Marks, X. Chen, R. Wu, R. B. Rashid, W. Jin, B. D. Paulsen, M. Moser, X. Ji, S. Griggs, D. Meli, X. Wu, H. Bristow, J. Strzalka, N. Gasparini, G. Costantini, S. Fabiano, J. Rivnay, I. McCulloch, *J. Am. Chem. Soc.* **2022**, *144*, 4642–4656.

[22] M. Alsufyani, M.-A. Stoeckel, X. Chen, K. Thorley, R. K. Hallani, Y. Puttisong, X. Ji, D. Meli, B. D. Paulsen, J. Strzalka, K. Regeta, C. Combe, H. Chen, J. Tian, J. Rivnay, S. Fabiano, I. McCulloch, *Angew. Chem. Int. Ed.* **2022**, *61*, e202113078.

[23] a) J. Han, H. Fan, Q. Zhang, Q. Hu, T. P. Russell, H. E. Katz, *Adv. Funct. Mater.* **2021**, *31*, 2005901; b) X. Yan, M. Xiong, X.-Y. Deng, K.-K. Liu, J.-T. Li, X.-Q. Wang, S. Zhang, N. Prine, Z. Zhang, W. Huang, Y. Wang, J.-Y. Wang, X. Gu, S. K. So, J. Zhu, T. Lei, *Nat. Commun.* **2021**, *12*, 5723; c) C. Y. Yang, W. L. Jin, J. Wang, Y. F. Ding, S. Nong, K. Shi, Y. Lu, Y. Z. Dai, F. D. Zhuang, T. Lei, C. A. Di, D. Zhu, J. Y. Wang, J. Pei, *Adv. Mater.* **2018**, *30*, 1802850; d) K. Feng, W. Shan, J. Wang, J.-W. Lee, W. Yang, W. Wu, Y. Wang, B. J. Kim, X. Guo, H. Guo, *Adv. Mater.* **2022**, *34*, 2201340.

[24] X. Yan, M. Xiong, J. T. Li, S. Zhang, Z. Ahmad, Y. Lu, Z. Y. Wang, Z. F. Yao, J. Y. Wang, X. Gu, T. Lei, *J. Am. Chem. Soc.* **2019**, *141*, 20215–20221.

[25] K. Shi, F. Zhang, C. A. Di, T. W. Yan, Y. Zou, X. Zhou, D. Zhu, J. Y. Wang, J. Pei, *J. Am. Chem. Soc.* **2015**, *137*, 6979–6982.

[26] K. Feng, H. Guo, J. Wang, Y. Shi, Z. Wu, M. Su, X. Zhang, J. H. Son, H. Y. Woo, X. Guo, *J. Am. Chem. Soc.* **2021**, *143*, 1539–1552.

[27] Y. Lu, Z.-D. Yu, H.-I. Un, Z.-F. Yao, H.-Y. You, W. Jin, L. Li, Z.-Y. Wang, B.-W. Dong, S. Barlow, E. Longhi, C.-a. Di, D. Zhu, J.-Y. Wang, C. Silva, S. R. Marder, J. Pei, *Adv. Mater.* **2021**, *33*, 2005946.

[28] J. Han, E. Tiernan, T. Lee, A. Chiu, P. McGuiggan, N. Adams, J. A. Tomko, P. E. Hopkins, S. M. Thon, J. D. Tovar, H. E. Katz, *Adv. Mater.* **2022**, *34*, 2201062.

[29] A. M. Nardes, M. Kemerink, R. A. J. Janssen, J. A. M. Bastiaansen, N. M. M. Kiggen, B. M. W. Langeveld, A. J. J. M. van Breemen, M. M. de Kok, *Adv. Mater.* **2007**, *19*, 1196–1200.

[30] K. Xu, H. Sun, T.-P. Ruoko, G. Wang, R. Kroon, N. B. Kolhe, Y. Puttisong, X. Liu, D. Fazzi, K. Shibata, C.-Y. Yang, N. Sun, G. Persson, A. B. Yankovich, E. Olsson, H. Yoshida, W. M. Chen, M. Fahlman, M. Kemerink, S. A. Jenekhe, C. Müller, M. Berggren, S. Fabiano, *Nat. Mater.* **2020**, *19*, 738–744.

[31] C.-Y. Yang, M.-A. Stoeckel, T.-P. Ruoko, H.-Y. Wu, X. Liu, N. B. Kolhe, Z. Wu, Y. Puttisong, C. Musumeci, M. Massetti, H. Sun, K. Xu, D. Tu, W. M. Chen, H. Y. Woo, M. Fahlman, S. A. Jenekhe, M. Berggren, S. Fabiano, *Nat. Commun.* **2021**, *12*, 2354.

[32] X. Yan, M. Xiong, X.-Y. Deng, K.-K. Liu, J.-T. Li, X.-Q. Wang, S. Zhang, N. Prine, Z. Zhang, W. Huang, Y. Wang, J.-Y. Wang, X. Gu, S. K. So, J. Zhu, T. Lei, *Nat. Commun.* **2021**, *12*, 5723.

[33] B. D. Naab, X. Gu, T. Kurosawa, J. W. F. To, A. Salleo, Z. Bao, *Adv. Electron. Mater.* **2016**, *2*, 1600004.
[34] O. Bardagot, C. Aumaître, A. Monmagnon, J. Pécaut, P.-A. Bayle, R. Demadrille, *Appl. Phys. Lett.* **2021**, *118*, 203904.
[35] I. E. Jacobs, Y. Lin, Y. Huang, X. Ren, D. Simatos, C. Chen, D. Tjhe, M. Statz, L. Lai, P. A. Finn, W. G. Neal, G. D'Avino, V. Lemaur, S. Fratini, D. Beljonne, J. Strzalka, C. B. Nielsen, S. Barlow, S. R. Marder, I. McCulloch, H. Sirringhaus, *Adv. Mater.* **2022**, *34*, 2102988.
[36] J. L. Bredas, G. B. Street, *Acc. Chem. Res.* **1985**, *18*, 309–315.
[37] S. A. Jenekhe, L. Lu, M. M. Alam, *Macromolecules* **2001**, *34*, 7315–7324.
[38] C. E. Tait, A. Reckwitz, M. Arvind, D. Neher, R. Bittl, J. Behrends, *Phys. Chem. Chem. Phys.* **2021**, *23*, 13827–13841.
[39] S.-J. Wang, D. Venkateshvaran, M. R. Mahani, U. Chopra, E. R. McNellis, R. Di Pietro, S. Schott, A. Wittmann, G. Schweicher, M. Cubukcu, K. Kang, R. Carey, T. J. Wagner, J. N. M. Siebrecht, D. P. G. H. Wong, I. E. Jacobs, R. O. Aboljadayel, A. Ionescu, S. A. Egorov, S. Mueller, O. Zadvorna, P. Skalski, C. Jellett, M. Little, A. Marks, I. McCulloch, J. Wunderlich, J. Sinova, H. Sirringhaus, *Nat. Electron.* **2019**, *2*, 98–107.
[40] a) X. Guo, A. Facchetti, *Nat. Mater.* **2020**, *19*, 922–928; b) T. O. Poehler, H. E. Katz, *Energy Environ. Sci.* **2012**, *5*, 8110–8115.
[41] F. Neese, *WIREs Comput. Mol. Sci.* **2012**, *2*, 73–78.
[42] X. Zhao, D. Madan, Y. Cheng, J. Zhou, H. Li, S. M. Thon, A. E. Bragg, M. E. DeCoster, P. E. Hopkins, H. E. Katz, *Adv. Mater.* **2017**, *29*, 1606921.
[43] H.-I. Un, S. A. Gregory, S. K. Mohapatra, M. Xiong, E. Longhi, Y. Lu, S. Rigin, S. Jhulki, C.-Y. Yang, T. V. Timofeeva, J.-Y. Wang, S. K. Yee, S. Barlow, S. R. Marder, J. Pei, *Adv. Energy Mater.* **2019**, *9*, 1900817.
[44] a) D. Curcó, C. Alemán, *J. Comput. Chem.* **2007**, *28*, 1743–1749; b) E. D. Miller, M. L. Jones, M. M. Henry, P. Chery, K. Miller, E. Jankowski, *Polymer* **2018**, *10*, 1305.
[45] C. De Rosa, G. Guerra, V. Petraccone, B. Pirozzi, *Macromolecules* **1997**, *30*, 4147–4152.
[46] I. E. Jacobs, G. D'Avino, V. Lemaur, Y. Lin, Y. Huang, C. Chen, T. F. Harrelson, W. Wood, L. J. Spalek, T. Mustafa, C. A. O'Keefe, X. Ren, D. Simatos, D. Tjhe, M. Statz, J. W. Strzalka, J.-K. Lee, I. McCulloch, S. Fratini, D. Beljonne, H. Sirringhaus, *J. Am. Chem. Soc.* **2022**, *144*, 3005–3019.
[47] Z. Ni, H. Dong, H. Wang, S. Ding, Y. Zou, Q. Zhao, Y. Zhen, F. Liu, L. Jiang, W. Hu, *Adv. Mater.* **2018**, *30*, 1704843.

Manuscript received: January 1, 2023
Accepted manuscript online: April 6, 2023
Version of record online: April 26, 2023